Available online at www.sciencedirect.com
ScienceDirect
Ceramics International 36 (2010) 1831–1836
CERAMICS INTERNATIONAL
www.elsevier.com/locate/ceramint

Effect of citric acid content on synthesis of $LiNi_{1/3}Mn_{1/3}Co_{1/3}O_2$ and its electrochemical characteristics

Gurpreet Singh [a], Anjan Sil [a,*], Sudipto Ghosh [b], Amrish Panwar [b]

[a] Department of Metallurgical and Materials Engineering, Indian Institute of Technology Roorkee, Roorkee 247 667, India
[b] Department of Metallurgical and Materials Engineering, Indian Institute of Technology Kharagpur, Kharagpur 721 302, India

Received 30 April 2009; received in revised form 10 January 2010; accepted 14 March 2010
Available online 28 April 2010

Abstract

$LiNi_{1/3}Mn_{1/3}Co_{1/3}O_2$ has been synthesized using different citric acid (chelating agent) contents to study the effect on morphology and electrochemical characteristics of the powdered compound synthesized. The citric acid content is expressed as R' which is the ratio of citric acid to metal ions. The processing with large value of R' yields the powder having particle size of about 200 nm. X-ray diffraction (XRD) analysis shows the powder has single phase layered rhombohedral structure. First cycle coulombic efficiency of the powder prepared with $R' = 3$, is ~93% in the voltage range of 4.6–2.5 V.

Keywords: A. Sol–gel process; B. Electron microscopy; C. Electrical conductivity; E. Electrodes

1. Introduction

There has been a growing interest to develop lithium ion batteries (LIBs) for various applications such as in mobile phones, laptops, video cameras, personal digital assistant and currently in hybrid electric vehicles. This is due to their importance over other secondary (rechargeable) batteries such as lead acid, nickel cadmium and nickel metal hydride batteries. First initiation towards the launch of lithium batteries in the market was attempted about two decades ago in 1990–1991 by Sony energy corporation. The battery uses $LiCoO_2$ as cathode [1] and the materials like graphite or MCMB as anode in the form of LiC_6 [2]. Since then, lot of efforts have been made to develop stable, higher capacity, long cyclable, cost effective and environmental friendly cathode and anode materials for LIBs. $LiCoO_2$ which has the rhombohedral structure, is the ideal choice for the cathode material in LIBs. But due to the high cost and toxic nature, its use is restrictive in bulk application e.g. hybrid electric vehicles (HEVs). Materials such as $LiMnO_2$ [3], $LiNiO_2$ [4], $LiMn_2O_4$ [5], $LiFePO_4$ [6] and $LiNi_{1/3}Mn_{1/3}Co_{1/3}O_2$ [7] are currently being used as cathode materials. Nickel manganese oxides with or without cobalt are also potential cathode materials for advanced LIBs [8]. These materials can be used for attaining higher operating voltage range required for HEVs.

Among all the cathode materials mentioned above, $LiNi_{1/3}Mn_{1/3}Co_{1/3}O_2$ provides rechargeable capacities of ~160 mAh/g and ~200 mAh/g in the voltage ranges of 2.5–4.4 V and 2.8–4.6 V, respectively, with excellent rate-capability [8]. Two exothermic peaks with low intensities at 160 °C and 210 °C for charged $LiCoO_2$ and a peak with high intensity at 210 °C for charged $LiNiO_2$, are observed in DSC profiles, while low intensity exothermic and endothermic peaks are observed in $LiNi_{1/3}Mn_{1/3}Co_{1/3}O_2$. This shows that structural distortion is less in the compound $LiNi_{1/3}Mn_{1/3}Co_{1/3}O_2$, which justifies further its suitability for the use as cathode material [9]. It has been established that under normal conditions of charging and discharging, Mn in $LiNi_{1/3}Mn_{1/3}Co_{1/3}O_2$ exists in +4 oxidation state, thus avoiding Jahn–Teller effect which induces structural distortion in the compound. The oxidation states of Co and Ni in the compound are +3 and +2 respectively. The successful use of $LiNi_{1/3}Mn_{1/3}Co_{1/3}O_2$ as cathode material in lithium ion battery at elevated temperature has been investigated owing to the fact that this material is used at higher voltage, which might lead to the increase in internal temperature of the battery. The

* Corresponding author. Tel.: +91 1332 285073; fax: +91 1332 285243/273560.
E-mail address: anj_sil@yahoo.co.uk (A. Sil).

0272-8842/$36.00
doi:10.1016/j.ceramint.2010.03.028

structural, electrochemical performance and morphology of the material depends on the synthesis route. The particle morphology and discharge profile of the materials depend severely on the synthesis route [10].

The synthesis of the cathode materials such as $LiMn_2O_4$, $LiCoO_2$ and $LiFePO_4$ using sol–gel technique has been reported by many researchers [11,12]. The synthesis of $LiNi_{1/3}Mn_{1/3}Co_{1/3}O_2$ by sol–gel method using different chelating agents viz. citric acid and polymer has also been reported [8,13,14]. The morphological control of the powder by the nature and quantity of chelating agent has been investigated and reported for $LiMn_2O_4$ [15]. However, to the best of authors' knowledge, the effect of chelating agent content such as citric acid on the powder morphology and its relation with electrical and electrochemical properties has not been reported so far for $LiNi_{1/3}Mn_{1/3}Co_{1/3}O_2$ synthesis. In the present study, the effect of citric acid content on the powder morphology and electrochemical characteristics of $LiNi_{1/3}Mn_{1/3}Co_{1/3}O_2$ has been investigated. The synthesized materials were characterized by using X-ray diffraction analysis, field emission scanning electron microscopy (FESEM), energy dispersive X-ray analysis (EDX), and impedance spectroscopy (IS). Electrochemical characteristics were studied in two different voltage windows of (i) 4.3–3.0 V and (ii) 4.6–2.5 V for commercial application and to examine extended structural stability of the material. Smaller particle size and higher coulombic efficiency of $LiNi_{1/3}Mn_{1/3}Co_{1/3}O_2$ have been achieved in the present study compared to the earlier studies reported on sol–gel synthesis of $LiNi_{1/3}Mn_{1/3}Co_{1/3}O_2$ [13,14].

2. Experimental

$LiNi_{1/3}Mn_{1/3}Co_{1/3}O_2$ samples were prepared using appropriate quantities of $Li(CH_3COO)\cdot H_2O$ (LOBA CHEMIE, 99%), $Ni(CH_3COO)_2\cdot 4H_2O$ (MERCK, $\geq$99.5%), $Mn(CH_3COO)_2\cdot 4H_2O$ (MERCK, $\geq$99.5%) and $Co(NO_3)_2\cdot 4H_2O$ (MERCK, $\geq$99%). Saturated solutions of these materials were prepared separately in distilled water and mixed with saturated solution of citric acid. The pH of the resultant solution mixture was maintained at about 9.0 by adding ammonium hydroxide solution. The mixture solutions were prepared for three different R' of 1, 2, and 3; where R' is the ratio of citric acid to metal ions. Viscous gel was obtained by stirring the solution maintained at temperature of 80–90 °C. The gel was heated in air to 450 °C for 5 h inside a furnace and then cooled in it. The precursor thus obtained was ground and calcined at 850 °C for 18 h in air followed by cooling to room temperature.

XRD patterns of the calcined powders were obtained by X-ray diffractometer (Philips PW3040/60) using Co Kα radiation of wavelength 1.78 Å in conjunction with iron filter. The scanning was made over $2\theta = 10–90°$, with a step size and dwell time of 0.1° and 5 s respectively.

Phase identification was carried out and the lattice parameters were determined using X'Pert High Score Plus software. Microstructural observations of the powder were made using FESEM (Supra 40 Carl ZEISS). Energy dispersive X-ray analysis (EDX) was also carried out along with the FESEM analysis to estimate bulk composition of the calcined powder.

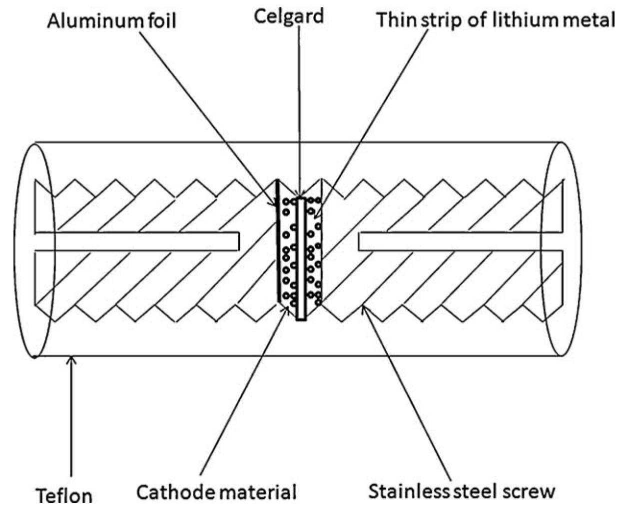

Fig. 1. Raw cell testing arrangement using teflon-stainless steel screw sample holder.

Electrical conductivities of the samples as a function of temperature were determined by impedance spectroscopy. The impedance measurements were made at a regular temperature interval of 25 °C in the temperature range of room temperature to 150 °C using impedance analyzer (Agilent 4294 A) operating in the frequency range of 40 Hz to 5 MHz. The samples were prepared from the powders in the form of cylindrical pellets of 10 mm diameter at a pressure level of 3 tonnes. For developing ohmic contact, silver paste was applied on the flat surfaces of the samples and dried at 120 °C for 24 h. Activation energy for migration of charge carriers was calculated from the temperature dependent conductivity plots. Electrochemical studies on the samples were performed in a teflon-stainless steel screw raw cell testing arrangement, which is shown in a schematic diagram (Fig. 1). The calcined powder was mixed with acetylene black and polyvinylidene fluoride (PVDF) in the ratio of 70:15:15 (wt%) and a slurry of the mixture was prepared in N-methylpyrrolidone (NMP). The slurry was applied on an aluminum foil by a blade and dried at a temperature of 120 °C for 24 h in an oven. Electrodes of about 1 cm^2 area were punched out of the foil. The reference electrode, separator and the electrolyte used were lithium metal strip, Celgard (2400) and 1 M $LiPF_6$/(EC + DEC) (1:1, v/v) respectively. Cells for all the cathode samples were charged and discharged at a constant current density of 100 μA-cm^{-2} in voltage ranges of 4.3–3.0 V and 4.6–2.5 V.

3. Results and discussion

XRD patterns of all the three powdered samples prepared by maintaining R' = 1, 2, and 3 are shown in Fig. 2, which shows that the XRD patterns of $LiNi_{1/3}Mn_{1/3}Co_{1/3}O_2$ are quite similar to that of single phase $LiCoO_2$ and $LiNiO_2$ as reported in the literature [1,4]. The materials have single phase layered rhombohedral structure with space group of R3m. This indicates that single phase of the compound can be obtained

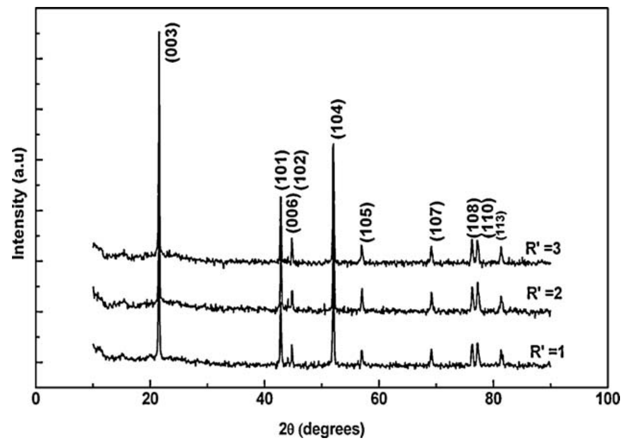

Fig. 2. XRD patterns of $LiNi_{1/3}Mn_{1/3}Co_{1/3}O_2$ powders synthesized for $R' = 1$, 2 and 3.

for all the concentrations of citric acid used. The lattice parameters of the unit cell of $LiNi_{1/3}Mn_{1/3}Co_{1/3}O_2$ for all R' values were obtained by Rietveld refinement of the respective XRD patterns. Background elimination and stripping of the peaks due to $CoK\alpha_2$ have been done to perform the refinement. The refined parameters are given in Tables 1a and 1b. It can be seen from Table 1a that the lattice parameter '*a*' is nearly same for all the three values of R', while no significant change in the '*c*' for different R' values has been resulted. The refined patterns along with difference plots are shown in Fig. 3. FESEM micrographs of all the three powdered samples are shown in Fig. 4 which shows that the average particle size increases from 250 nm to 400 nm as R' changes from 1 to 2. The average particle size becomes 200 nm for $R' = 3$. This is presumably due to the fact that at $R' = 3$ nucleation rate dominates growth rate leading to the formation of smaller particles. The decrease in particle size implies the increase in surface area to volume ratio of the particle in the case of $R' = 3$. The morphology of the particles is found to be truncated octahedron in all the samples studied. The overall size of the powder particles considering all the three cases of R', ranges from 100 nm to 500 nm. In the case of $R' = 2$, some particles are larger in size. The particle size reported for the compound $LiNi_{1/3}Mn_{1/3}Co_{1/3}O_2$ synthesized by sol–gel process [13] is 1–3 μm, which is larger than that obtained in the present study.

Table 1a
Refined parameters: lattice parameters and agreement indices for $LiNi_{1/3}Mn_{1/3}Co_{1/3}O_2$.

R'	Lattice parameters		c/a	Agreement indices (%)			
	a (Å)	c (Å)		Rex	Rp	Rwp	GOF
1	2.8617(1)	14.251(2)	4.9799	3.14	2.87	3.66	1.35
2	2.8617(2)	14.242(2)	4.9767	3.02	2.83	3.62	1.44
3	2.8620(3)	14.254(2)	4.9804	3.10	2.94	3.71	1.43

Table 1b
Occupancy and atomic fraction coordinates for $LiNi_{1/3}Mn_{1/3}Co_{1/3}O_2$ for $R' = 3$.

Atom	Wyckoff position	Site occupancy factor	x	y	z
Li1	3a	0.966300	0.000000	0.000000	0.000000
Ni1	3a	0.033700	0.000000	0.000000	0.000000
Li2	3b	0.033700	0.000000	0.000000	0.500000
Ni2	3b	0.299600	0.000000	0.000000	0.500000
Mn	3b	0.333300	0.000000	0.000000	0.500000
Co	3b	0.333300	0.000000	0.000000	0.500000
O	6c	1.000000	0.000000	0.000000	0.241300

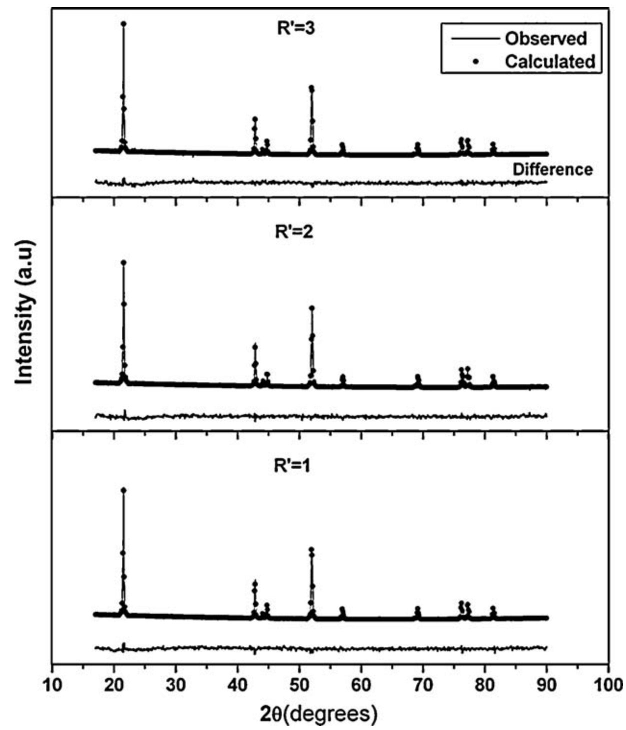

Fig. 3. Refined XRD patterns $LiNi_{1/3}Mn_{1/3}Co_{1/3}O_2$ powders synthesized for $R' = 1$, 2 and 3.

Fig. 5 shows the results of EDX analysis conducted in the area scan mode for the various samples. The compositions in atomic percent of Ni, Mn, Co and O in the samples are given in Table 2. Li being low atomic number element is not detectable by the EDX scan and has been eliminated in the compositional determinations. It can be examined from the Table 2 that the powders processed with $R' = 1$ and 3, have compositions close to stoichiometry, though there is a slight deviation from ideal stoichiometry for the powders synthesized with $R' = 2$.

Impedance measurements on various samples were made to determine the bulk impedance of the material. Bulk impedance was calculated by plotting real and imaginary parts of the impedance data in a complex plane as shown in Fig. 6. Electrical conductivity (dc) of the samples has been calculated from the resistance values obtained by extrapolation of the impedance data and from the intersection on the X-axis, taken over room temperature to 150 °C at an interval of 25 °C. The intercept of the semicircular arc in the lower frequency on the X-axis gives the bulk resistance. The electrical conductivity (σ) of the samples is calculated from the following relation:

$$\sigma = \left(\frac{1}{R}\right) \times \left(\frac{l}{A}\right)$$

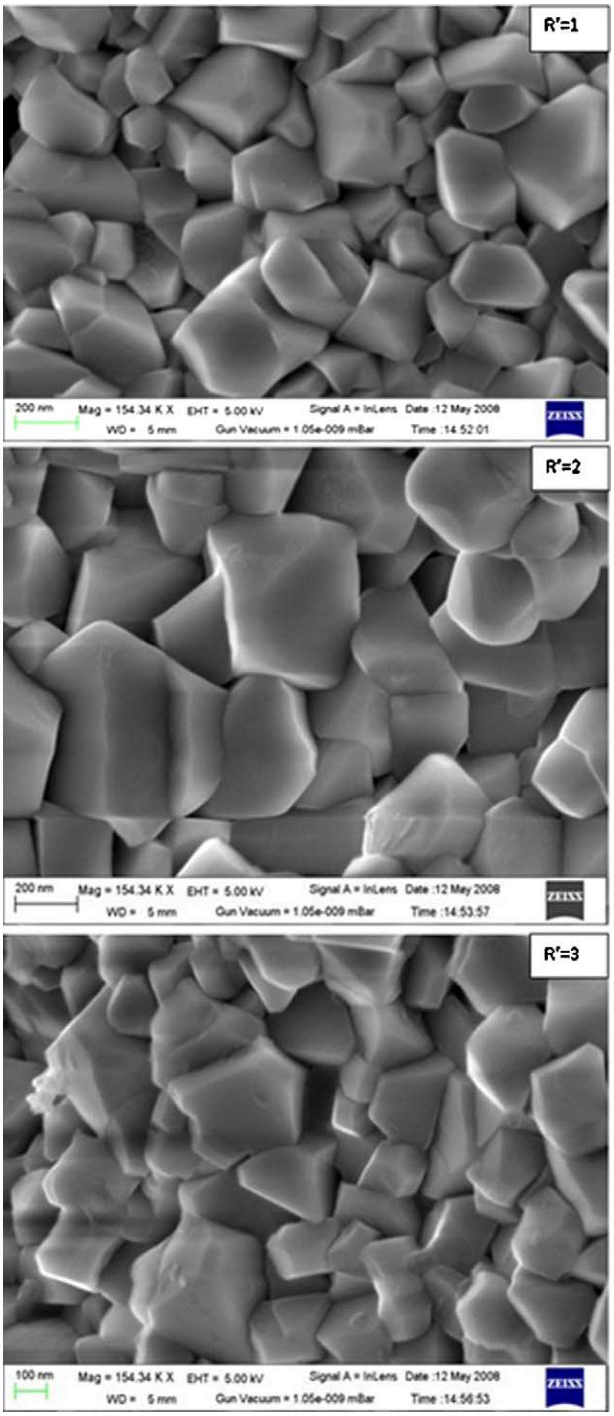

Fig. 4. FESEM micrographs of $LiNi_{1/3}Mn_{1/3}Co_{1/3}O_2$ powders for $R' = 1$, 2 and 3.

where R is the bulk resistance, l the thickness and A the area of the flat surface of the cylindrical sample. The variation of the electrical conductivity with temperature is shown in Fig. 7. The electrical conductivity of the materials as a function of temperature T can be described by using following relation:

$$\sigma = \sigma_0 \exp\left(\frac{-E_a}{KT}\right)$$

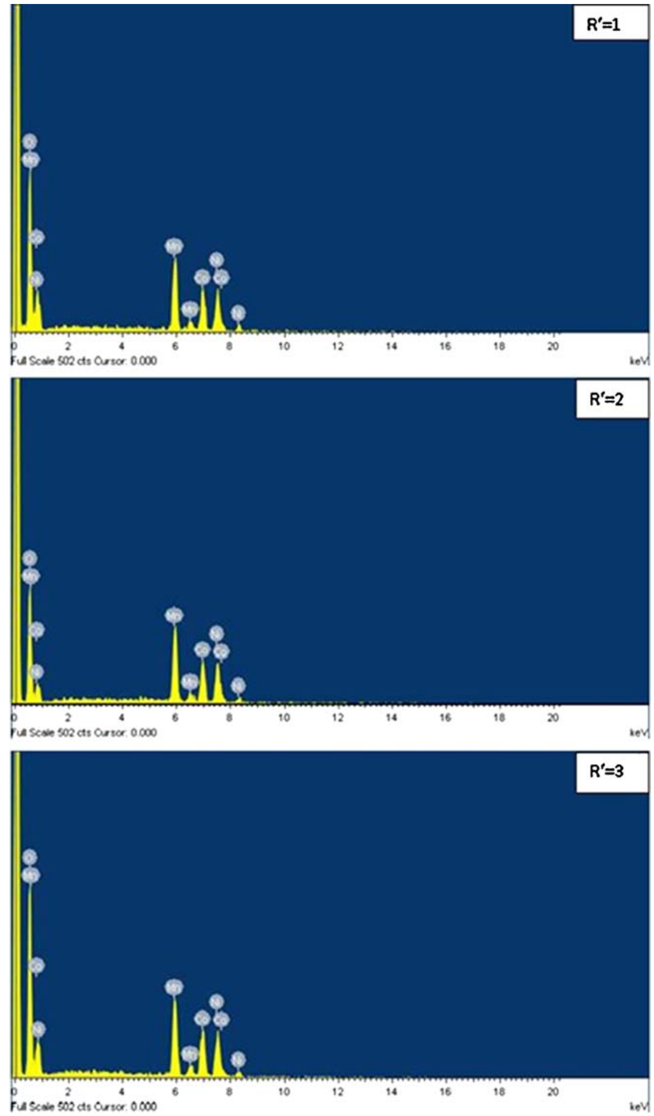

Fig. 5. EDX analysis of $LiCo_{1/3}Ni_{1/3}Mn_{1/3}O_2$.

where σ_0, E_a and K are the pre exponential factor, activation energy of mobile charge carrier and Boltzmann constant respectively. E_a was calculated from the slope of the graph between log(σ) and 1000/T. E_a is approximately same for all the samples and the values are 0.38 eV, 0.37 eV and 0.39 eV for $R' = 1$, 2 and 3 respectively. The electrical conductivity at room temperature

Table 2
Atomic % of O, Mn, Co and Ni present (ignoring the Li content) in three different samples as shown by EDX analysis.

Element	Atomic (%)			
	Calculated for $LiNi_{1/3}Mn_{1/3}Co_{1/3}O_2$	Determined for $R' = 1$	$R' = 2$	$R' = 3$
O	50.00	66.49	60.32	67.85
Mn	8.33	12.43	14.30	11.00
Co	8.33	9.98	12.44	9.96
Ni	8.33	11.11	12.93	11.19
Li	25.00	–	–	–

(–), not determined.

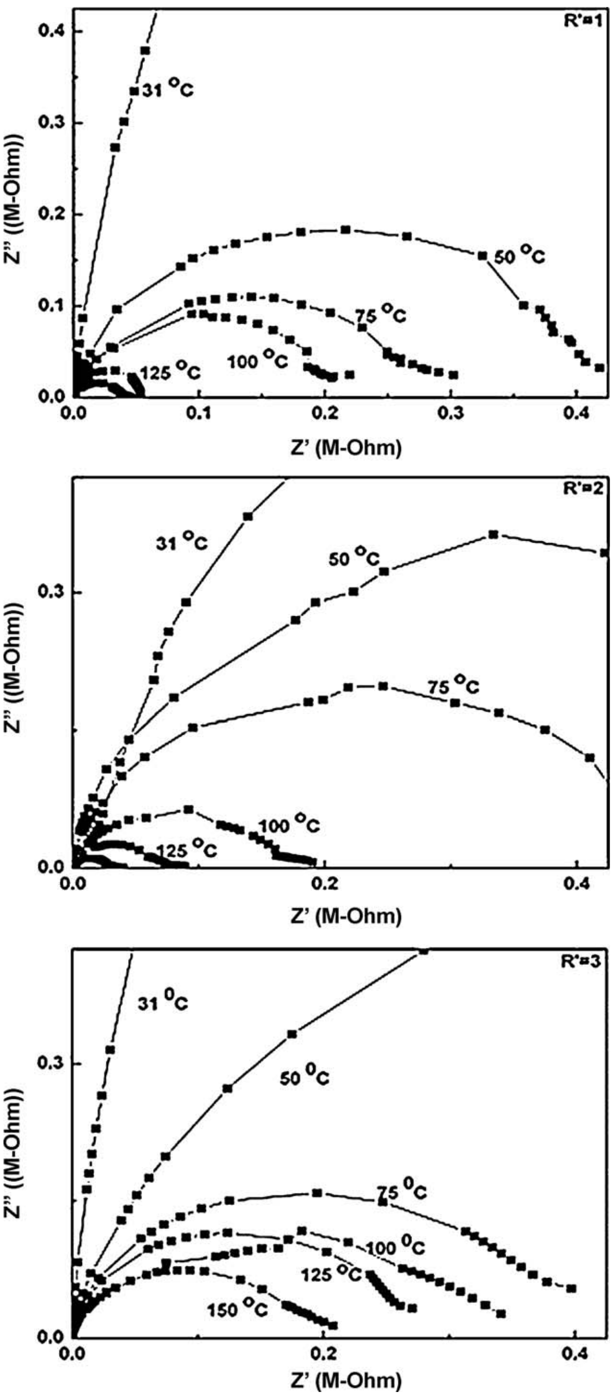

Fig. 6. Complex impedance plots for $LiCo_{1/3}Ni_{1/3}Mn_{1/3}O_2$ synthesized with $R' = 1$, 2 and 3.

for the various samples is in the range of 10^{-7}–10^{-8} S/cm. In $LiNi_{1/3}Mn_{1/3}Co_{1/3}O_2$, the electronic configurations of Mn^{4+}, Co^{3+} and Ni^{2+} are ($t_{2g}^3e_g^0$), ($t_{2g}^6e_g^0$), and ($t_{2g}^6e_g^2$) respectively. Due to the absence of free charge carriers, no effective transport can take place. Hence low electrical conductivities and high activation energies are resulted. These results are in agreement with the earlier studies reported [16].

Electrochemical measurements were made on various samples for $R' = 1$, 2 and 3 in a voltage range of 4.3–3.0 V. Discharge curves for the various samples are shown in Fig. 8,

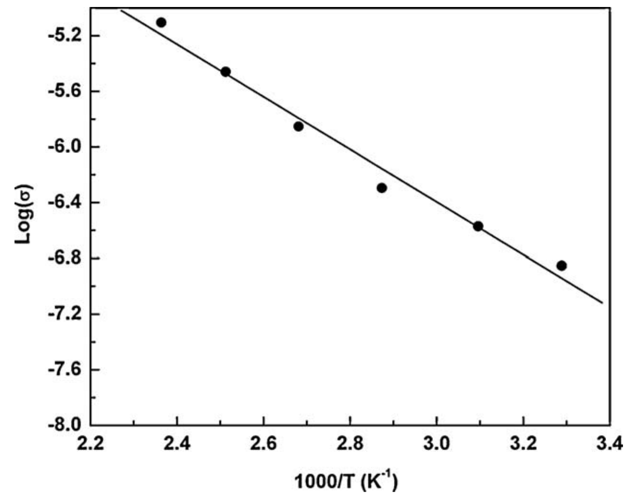

Fig. 7. Plot of log(σ) vs. 1000/T for $LiCo_{1/3}Ni_{1/3}Mn_{1/3}O_2$ synthesized with $R' = 2$.

which shows that the materials of all compositions have almost same discharge capacities which are 146.15 mAh/g, 153.76 mAh/g and 151.76 mAh/g for $R' = 1$, 2 and 3 respectively. From all three discharge curves it was found that the behavior of discharge is same as reported earlier [8]. The electrochemical performance of the material for $R' = 3$ was studied for 8 cycles over a wide voltage range of 2.5–4.6 V and the result is shown in Fig. 9. The discharge capacity for the first cycle to next cycle decreases from 200.67 mAh/g to 189.42 mAh/g, which indicates that during first charge of sample a proportion of Li inserted to anode may not be reinserted back to cathode during the subsequent discharge because of irreversible internal chemical reactions [17]. It has been reported [8] that irreversible capacity of $Li_xNi_{1/3}Mn_{1/3}Co_{1/3}O_2$ is required to be reduced for a full scale commercial exploitation of such cathode material. The irreversible capacities of the $LiNi_{1/3}Mn_{1/3}Co_{1/3}O_2$ material synthesized at 800 °C and 900 °C by sol–gel route are 36 mAh/g and

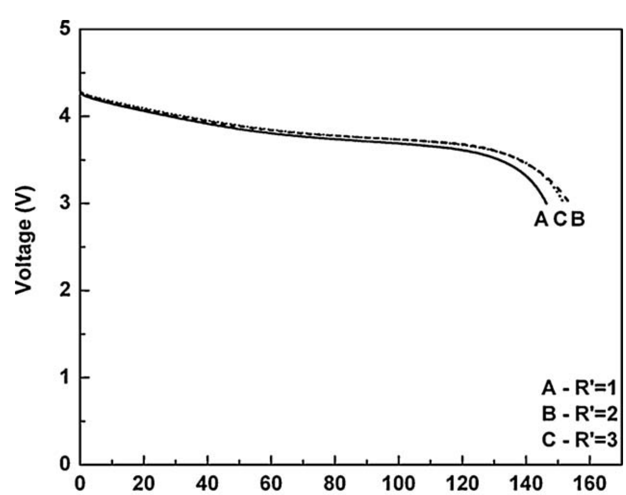

Fig. 8. First discharge curves of $LiCo_{1/3}Ni_{1/3}Mn_{1/3}O_2$ for $R' = 1$, 2 and 3 in a voltage range of 4.3–3.0 V.

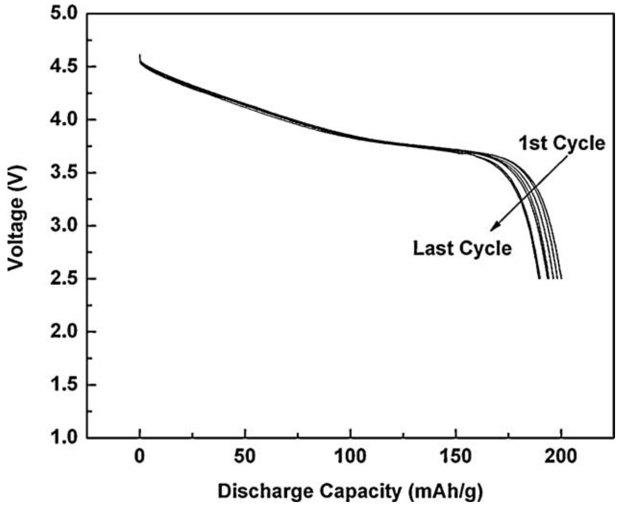

Fig. 9. Discharge curves for the first 8 cycles of $LiCo_{1/3}Ni_{1/3}Mn_{1/3}O_2$ for $R' = 3$ in a voltage range of 4.6–2.5 V.

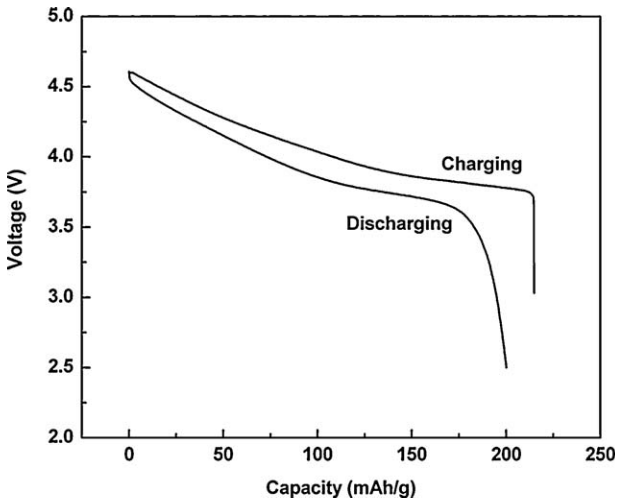

Fig. 10. First charge–discharge cycle of $LiCo_{1/3}Ni_{1/3}Mn_{1/3}O_2$ for $R' = 3$ in the voltage range of 4.6–2.5 V.

24 mAh/g respectively [8]. Some other studies on the sol–gel synthesis of $LiNi_{1/3}Mn_{1/3}Co_{1/3}O_2$ have shown the coulombic efficiency of 87.3% when cell was cycled at 100 μA-cm^{-2} in the potential range of 2.8–4.5 V [14]. The present study shows higher coulombic efficiency of 93%, as shown in Fig. 10, for $R' = 3$ when cell cycles at a rate of 100 μA-cm^{-2} in the potential range of 2.5–4.6 V.

4. Conclusions

Following conclusions can be drawn from the present study:

(1) Single phase layered rhombohedral structure of $LiNi_{1/3}Mn_{1/3}Co_{1/3}O_2$ can be obtained using sol–gel synthesis with various content of chelating agent citric acid.
(2) The synthesis with higher citric acid content yields 200 nm sized powder, the size is smaller than 1–3 μm reported [14].
(3) Powders processed with $R' = 1$ and 3, have compositions close to stoichiometry, though there is a slight deviation from ideal stoichiometry for the powders synthesized with $R' = 2$.
(4) The activation energy for conduction is same for all the samples processed with various citric acid content.
(5) The first cycle coulombic efficiency for $R' = 3$ in the voltage range of 4.6–2.5 V is 93%, whereas, the efficiency reported so far [14] in the voltage range of 4.6–2.8 V is 87.3% using sol–gel technique. The first cycle discharge capacities for $R' = 1$, 2 and 3 are 146.15 mAh/g, 153.76 mAh/g and 151.76 mAh/g respectively in the voltage range of 4.3–3.0 V. A discharge capacity of 200 mAh/g has been observed for $R' = 3$ in the voltage range of 4.6–2.5 V.

References

[1] K. Mizushima, P.C. Jones, P.J. Wiseman, J.B. Goodenough, Li_xCoO_2 ($0 < x \leq 1$): a new cathode material for batteries of high energy density, Mat. Res. Bull. 15 (6) (1980) 783–789.
[2] Samar Basu, U.S.Patent, 4,423,125, 27 December, 1983.
[3] I.J. Davidson, R.S. McMillan, J.J. Murray, J.E. Greedan, Lithium-ion cell based on orthorhombic $LiMnO_2$, J. Power Sources 54 (2) (1995) 232–235.
[4] T. Thongtem, S. Thongtem, Synthesis of $Li_{1-x}Ni_{1+x}O_2$ using malonic acid as a chelating agent, Ceram. Int. 31 (2) (2005) 241–247.
[5] M.M. Thackeray, W.I.F. David, P.G. Bruce, J.B. Goodenough, Lithium insertion into manganese spinels, Mat. Res. Bull. 18 (4) (1983) 461–472.
[6] A.K. Padhi, K.S. Nanjundaswamy, J.B. Goodenough, Phospho-olivines as positive-electrode materials for rechargeable lithium batteries, J. Electrochem. Soc. 144 (4) (1997) 1188–1194.
[7] T. Ohzuku, Y. Makimura, Layered lithium insertion material of $LiCo_{1/3}Ni_{1/3}Mn_{1/3}O_2$ for lithium-ion batteries, Chem. Lett. 30 (7) (2001) 642–643.
[8] B.J. Hwang, Y.W. Tsai, D. Carlier, G. Ceder, A combined computational/experimental study on $LiNi_{1/3}Co_{1/3}Mn_{1/3}O_2$, Chem. Mater. 15 (19) (2003) 3676–3682.
[9] N. Yabuuchi, T. Ohzuku, Novel lithium insertion material of $LiCo_{1/3}Ni_{1/3}Mn_{1/3}O_2$ for advanced lithium-ion batteries, J. Power Sources 119–121 (2003) 171–174.
[10] D.-C. Li, T. Muta, L.-Q. Zhang, M. Yoshio, H. Noguchi, Effect of synthesis method on the electrochemical performance of $LiNi_{1/3}Mn_{1/3}Co_{1/3}O_2$, J. Power Sources 132 (1–2) (2004) 150–155.
[11] Y. Sundarayya, K.C. Kumara Swamy, C.S. Sunandana, Oxalate based non-aqueous sol–gel synthesis of phase pure sub-micron $LiFePO_4$, Mat. Res. Bull. 42 (11) (2007) 1942–1948.
[12] P. Barboux, J.M. Tarascon, F.K. Shokoohi, The use of acetates as precursors for the low-temperature synthesis of $LiMn_2O_4$ and $LiCoO_2$ intercalation compounds, J. Solid State Chem. 94 (1) (1991) 185–196.
[13] J. Hong, B. Fang, C. Wang, The electrochemical performance of $LiNi_{1/3}Mn_{1/3}Co_{1/3}O_2$ prepared by sol–gel method, in: 211th ECS Meeting, vol. 89, 2007.
[14] M. Wang, F. Wu, Y.-f. Su, Synthesis and characterization of $LiCo_{1/3}Ni_{1/3}Mn_{1/3}O_2$ by an improved sol–gel method, J. Beijing Inst. Technol. 27 (Suppl. 2) (2007) 95–99.
[15] Y.-K. Sun, I.-H. Oh, K.Y. Kim, Synthesis of spinel $LiMn_2O_4$ by the sol–gel method for a cathode-active material in lithium secondary batteries, Ind. Eng. Chem. Res. 36 (11) (1997) 4839–4846.
[16] M. Gozu, K. Swierczek, J. Molenda, Structural and transport properties of layered $Li_{1+x}(Mn_{1/3}Co_{1/3}Ni_{1/3})_{1-x}O_2$ oxides prepared by a soft chemistry method, J. Power Sources 194 (2009) 38–44.
[17] M.Y. Song, J. Song, E. Bang, D.R. Mumm, Electrochemical properties of $LiNi_{1-y}Co_yO_2$ cathode materials synthesized from different starting materials by the solid-state reaction method, Ceram. Int. 35 (2009) 1625–1631.